NANO · MICRO small
www.small-journal.com

Slowing the Kinetics of Alumina Sol–Gel Chemistry for Controlled Catalyst Overcoating and Improved Catalyst Stability and Selectivity

*Yuan-Peng Du, Florent Héroguel, and Jeremy S. Luterbacher**

Catalyst overcoating is an emerging approach to engineer surface functionalities on supported metal catalyst and improve catalyst selectivity and durability. Alumina deposition on high surface area material by sol–gel chemistry is traditionally difficult to control due to the fast hydrolysis kinetics of aluminum-alkoxide precursors. Here, sol–gel chemistry methods are adapted to slow down these kinetics and deposit nanometer-scale alumina overcoats. The alumina overcoats are comparable in conformality and thickness control to overcoats prepared by atomic layer deposition even on high surface area substrates. The strategy relies on regulating the hydrolysis/condensation kinetics of $Al(^sBuO)_3$ by either adding a chelating agent or using nonhydrolytic sol–gel chemistry. These two approaches produce overcoats with similar chemical properties but distinct physical textures. With chelation chemistry, a mild method compatible with supported base metal catalysts, a conformal yet porous overcoat leads to a highly sintering-resistant Cu catalyst for liquid-phase furfural hydrogenation. With the nonhydrolytic sol–gel route, a denser Al_2O_3 overcoat can be deposited to create a high density of Lewis acid–metal interface sites over Pt on mesoporous silica. The resulting material has a substantially increased hydrodeoxygenation activity for the conversion of lignin-derived 4-propylguaiacol into propylcyclohexane with up to 87% selectivity.

1. Introduction

Supported metal catalysts are widely used in many commercial enterprises including petroleum refineries, emission control, pharmaceutical production and, increasingly, in biomass conversion. In the past, catalyst research focused on controlling metal particle size and screening suitable supports to enhance catalytic activities. As synthetic techniques increasingly allow us to control the material's nanoenvironment, the importance of catalyst structure and surface properties has begun to be recognized as it is found to be closely related to catalyst stability and selectivity.[1,2] Catalyst overcoating is an emerging postsynthesis modification strategy for engineering the surface nanostructure and functionality of various catalysts.[3,4] Many studies have reported improving the selectivities and stabilities of a variety of catalysts by depositing SiO_2 overcoats.[5–8] However, silica is not hydrothermally stable which has limited its use in renewable catalytic systems that generally feature aqueous conditions.[9,10] Catalytic systems featuring biomass-derived streams are one such category of reactions where the water content in plants and/or hydrolysis-based deconstruction processes lead to hydrothermal catalytic conversions. This has increased the interest in more hydrothermally stable oxides like alumina (Al_2O_3). Al_2O_3 deposition has also generated interest because the addition of its intrinsic Lewis acidity has a potential to create new active sites.[11,12]

Atomic layer deposition (ALD) is well known as an effective method for depositing alumina on substrate in either powder or film form and it has been widely applied to improve the performances of heterogeneous catalysts.[4,13–15] The greatest advantage of ALD is the highly controllable growth of the deposited overcoat with respect to thickness and uniformity.[16] However, ALD is hard to scale and requires a heavy instrumentation and the use of expensive gaseous precursors. In contrast, sol–gel methods are considered simpler and cheaper alternatives.[17] Nonetheless, depositing Al_2O_3 over nanoparticles with high surface areas via sol–gel process remains particularly challenging because of the high hydrolysis/condensation rate of aluminum alkoxides.[18] For instance, SiO_2 overcoating can be easily performed by applying the so-called "Stöber method," which is carried out by adding tetraethoxysilane (TEOS) into a suspension containing the substrate, a controlled amount of ethanol, ammonia, and water.[19] However, the same procedure with classic alumina precursors such as aluminum sec-butoxide ($Al(^sBuO)_3$) leads to the rapid formation of alumina precipitates.

In order to synthetize conformal overcoats with a controlled thickness and density using liquid phase sol–gel chemistry techniques, our main strategy was to tailor the condensation kinetics of an alumina precursor. We had previously explored nonhydrolytic sol–gel (NHSG) chemistry to deposit titania

Y.-P. Du, Dr. F. Héroguel, Prof. J. S. Luterbacher
Laboratory of Sustainable and Catalytic Processing
Institute of Chemical Sciences and Engineering
École Polytechnique Fédérale de Lausanne (EPFL)
CH-1015, Lausanne, Switzerland
E-mail: jeremy.luterbacher@epfl.ch

The ORCID identification number(s) for the author(s) of this article can be found under https://doi.org/10.1002/smll.201801733.

DOI: 10.1002/smll.201801733

(TiO_2) that has similar highly reactive precursors in aqueous media.[20] Currently, no NHSG methods exist for Al_2O_3 deposition on high surface area materials. On the other hand, ligands containing β-dicarbonyl groups, such as acetylacetone (AcAc) and ethyl acetoacetate (EAA) have also been reported to chelate with metal alkoxides by ligand substitution and slow down their high condensation rates. Although chelation chemistry methods have been previously applied for alumina deposition on thin films,[21,22] it has similarly not been used for high surface area powder samples such as those used in heterogeneous catalysis. Our objective was to develop a toolbox of alumina overcoating methods using these complementary methods that both slow down the kinetics of alumina condensation.

Here, we demonstrate that the sol–gel kinetics can be modified by nonhydrolytic sol–gel and chelation chemistry to achieve conformal alumina overcoats with controlled thicknesses of nanometer precision. Specifically, we report two Al_2O_3 deposition methods performed in liquid phase with $Al(^sBuO)_3$ which is an inexpensive and common precursor for alumina sol–gel processing. We applied said methods to overcoat two typical high surface area supported metal catalysts and demonstrate the complementary uses of both resulting catalysts in biomass conversion reactions, which lead to increased stability and activity, respectively.

2. Results and Discussions

2.1. Design of Al_2O_3 Precursors with Slower Hydrolysis/Condensation Kinetics

Our first strategy was chemically modifying $Al(^sBuO)_3$ based on NHSG chemistry of alumina, which was first reported by Acosta et al.[23] Typically, the precursor of the NHSG reaction can be prepared by mixing metal halides and metal alkoxides. Ligand exchange occurs between the metal halide and metal alkoxide at room temperature while condensation only takes place at higher temperatures. The gelation is likely initiated by the ligand exchanged precursors as shown in the previous studies of $TiCl_4$–$Ti(^iPrO)_4$ NHSG chemistry.[24] The actual precursors involved in those gelation processes have been identified as $Ti(^iPrO)_3Cl$ and $Al(^iPrO)_2Cl$ for $Ti(^iPrO)_4$–$TiCl_4$ and $Al(^iPrO)_3$–$AlCl_3$ pairs, respectively.[25] Mixing metal alkoxides and metal halides with nonoptimal ratios has been shown to cause long gelation time.[24] Therefore, the ratio of $Al(^sBuO)_3$ and $AlBr_3$ was kept to 2 by presuming that $Al(^sBuO)_3$–$AlBr_3$ route follows the same chemistry reported in the literature of analogous Ti and Al systems (**Figure 1**a).[25] $AlBr_3$ was preferred over $AlCl_3$ to allow using CH_2Br_2 as a solvent instead of the more toxic CCl_4.[23] The second strategy was adding EAA to chelate $Al(^sBuO)_3$ by ligand substitution.[18,26,27] The sol–gel kinetics of the resulting chelated alumina precursor and its associated gelation rate is dependent on the ratio between chelating agents and $Al(^sBuO)_3$. In this work, we prepared the precursor by reacting 0.75 equivalent EAA with $Al(^sBuO)_3$ (Figure 1a).

After preparing the precursors, the catalysts were either dispersed in a Stöber solution (chelated precursor) or a heated anhydrous CH_2Br_2 (NHSG precursors). Alumina deposition was systematically initiated by injecting the precursors into these respective suspensions. A syringe pump (Figure 1b) was used to inject the precursors and avoid any undesirable homogeneous condensation due to a high precursor concentration within the catalyst suspension.

In order to approximately estimate the amount of precursor needed to form a single atomic monolayer on the surface of the catalyst, we calculated the surface projection of the Van Der Waals volumes of the precursor molecules by MarvinSketch software (Figure 1c), which were estimated to be 0.48 and 1.0 nm^2 for $Al(^sBuO)Br_2$ and $Al(^sBuO)_2(EAA)$, respectively. Our past work with alumina has shown that steric hindrances between precursors is the determining factor for calculating maximum precursor coverage on the surface instead of hydroxyl density.[28] The necessary amount of precursor for achieving monolayer coverage on a specific material was then calculated by dividing the specific surface area of the catalyst by this projected precursor area. Knowing the amount of precursor needed to form a monolayer allows us to target a targeted number of deposited monolayers by controlling the total amount of injected precursor, leading to sub-nanometer control of the overcoat thickness.

2.2. Al_2O_3 Deposition by Chelation Chemistry

Al_2O_3 overcoating using the chelating method was first performed on SiO_2 spheres with relatively low specific surface area (as determined by the Brunauer–Emmett–Teller (BET) method as 15 $m^2\ g^{-1}$, S_{BET}) to easily image the overcoat. An amount of 40 monolayers coverage of $Al(^sBuO)_2(EAA)$ was deposited and the product was referred as C-Al_2O_3@SiO_2, where C denotes materials prepared using the chelation chemistry method. Though high-angle annular dark field scanning transmission electron microscopy (HAADF STEM) provides low contrast between the SiO_2 core and the Al_2O_3 shell (**Figure 2**a), energy dispersive X-ray (EDX) spectroscopy mapping clearly shows that a conformal alumina overcoat was formed on the silica spheres (Figure 2b) with an average thickness of 6.1 ± 2.0 nm. We subsequently investigated Al_2O_3 deposition on Pt supported on high surface area mesoporous silica (SBA-15), which is more representative of a material used for catalytic applications. The final injected amount of Al per unit weight of SBA-15 was 3.4 mmol $g_{catalyst}^{-1}$, which corresponded to approximately three monolayers of $Al(^sBuO)_2(EAA)$. Figure 2c,d shows no modification of SBA-15's morphology after alumina deposition (for comparison, a TEM image of the uncoated material is available in Figure S1, Supporting Information). EDX mapping (Figure 2e) showed a uniform distribution of Si and Al, which implied that Al_2O_3 growth occurred within the pore structure. Formation of the Al_2O_3 layer inside the pores was also supported by the measurement of a reduced average pore size (from 6.8 to 6.3 nm) as determined by nitrogen physisorption (Figure S2a, Supporting Information). Notably, the periodic hexagonal structure of SBA-15 was fully preserved after overcoating as evidenced by powder X-ray diffraction (XRD) (Figure S2b, Supporting Information). In agreement with previous work studying the surface alumination of SBA-15 and NHSG TiO_2 deposition, the S_{BET} of C-Al_2O_3@2%Pt/SBA-15 was drastically

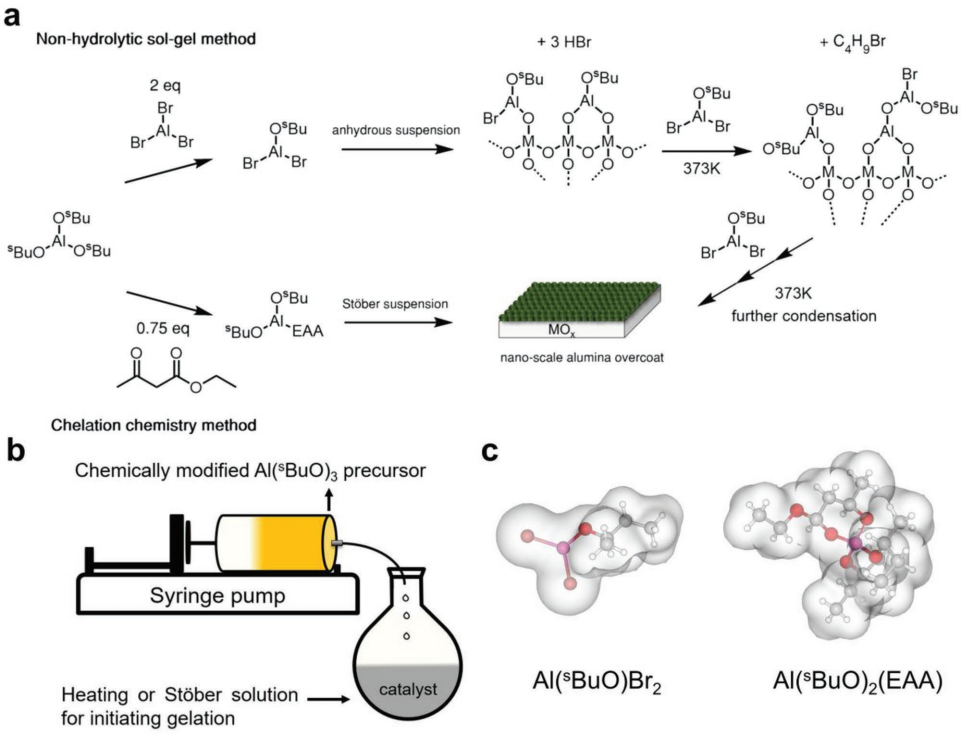

Figure 1. a) NHSG and chelation chemistry of $Al(^sBuO)_3$ for controlled Al_2O_3 deposition. b) Schematic illustration of the continuous injection syringe pump setup. c) Van Der Waals structure and the volumes of the two chemically modified $Al(^sBuO)_3$.

decreased, from 723 to 392 $m^2\ g^{-1}$, which has been determined as being linked to the filling of micropores.[20,29] Importantly, this method is not merely restricted to overcoating silica-based substrates. We successfully overcoated other metal oxides like Fe_2O_3 ellipsoid nanoparticles and even hydrophobic substrates such as carbon spheres (Figure S3, Supporting Information).

Previous attempts to overcoat Al_2O_3 on powder substrates by sol–gel based methods had been made by repeatedly grafting aluminum alkoxides with surface hydroxyl groups in anhydrous conditions.[29–31] Nonetheless, the overlayers in those studies did not uniformly grow over the surfaces or pore structures. We previously reported a new alumina overcoating method to control the condensation by stochiometrically controlling the H_2O amount but this method gave poor results when coating catalysts with S_{BET} above 150 $m^2\ g^{-1}$.[28] In contrast, the overcoat of C-Al_2O_3@SiO_2 was comparable in appearance and conformality to the alumina overcoat produced by ALD.[32] Another disadvantage of those published methods was that they required time-consuming multistep approaches to achieve thicker overcoats. However, this presented approach can be performed in a single step with an automated injection. Furthermore, it still produced high quality (e.g., uniform and conformal) overcoats when the amount of alumina loading was increased by five times (14 monolayer equivalents of precursor, sample denoted as C-5Al_2O_3@SBA-15, Figure S1a, Supporting Information). In this case, the average pore size of C-5Al_2O_3@SBA-15 was reduced to 4.1 nm while narrow pore size distributions as well as the characteristic diffraction peak of SBA-15 were still observed (Figure S2, Supporting Information). According to the pore size determined by physisorption, the thickness of the alumina overcoat in the pores (1.35 nm) was close to the predicted thickness based on the calculated thickness of one monolayer of alumina (1.25 nm for 14 monolayers, or 0.09 nm per monolayer estimated from C-Al_2O_3@2%Pt/SBA-15).

Several important parameters govern our chelation method. First, the quantity of added H_2O is crucial for controlling hydrolysis kinetics. The ratio of water and ethanol used in this work was much lower (0.04) than that present in the Stöber solution used for preparing spherical silica (0.15) because we observed that $Al(^sBuO)_2(EAA)$ still reacts with H_2O faster than tetraethoxysilane does. Nevertheless, an insufficient concentration of water hindered the gelation of precursor and so an appropriate balance was required. Second, the concentration of NH_3, which acts as a catalyst to initiate the hydrolysis and condensation of metal alkoxides, needs to be decreased when overcoating high surface area substrates with porous structures such as SBA-15. A high NH_3 concentration led to preferential condensation on the surface of SBA-15 particles before the precursor could diffuse into the pore structure. Figure S1b in the Supporting Information shows the image of overcoated SBA-15 prepared with an excess $NH_{3(aq)}$ (0.04 mL instead of 0.02 mL). The formation of fibrous structures around the particles was indicative of alumina growth outside of the catalyst pellet. Third, higher EAA/$Al(^sBuO)_3$ ratios are known to decrease gelation times.[21] Therefore, NH_3 and/or H_2O concentration had to be adjusted to obtain suitable gelation times when a higher EAA/$Al(^sBuO)_3$ ratio was used. These effects showed how the interplay of EAA binding, water, and ammonia can be used to control the sol–gel kinetics of $Al(^sBuO)_3$.

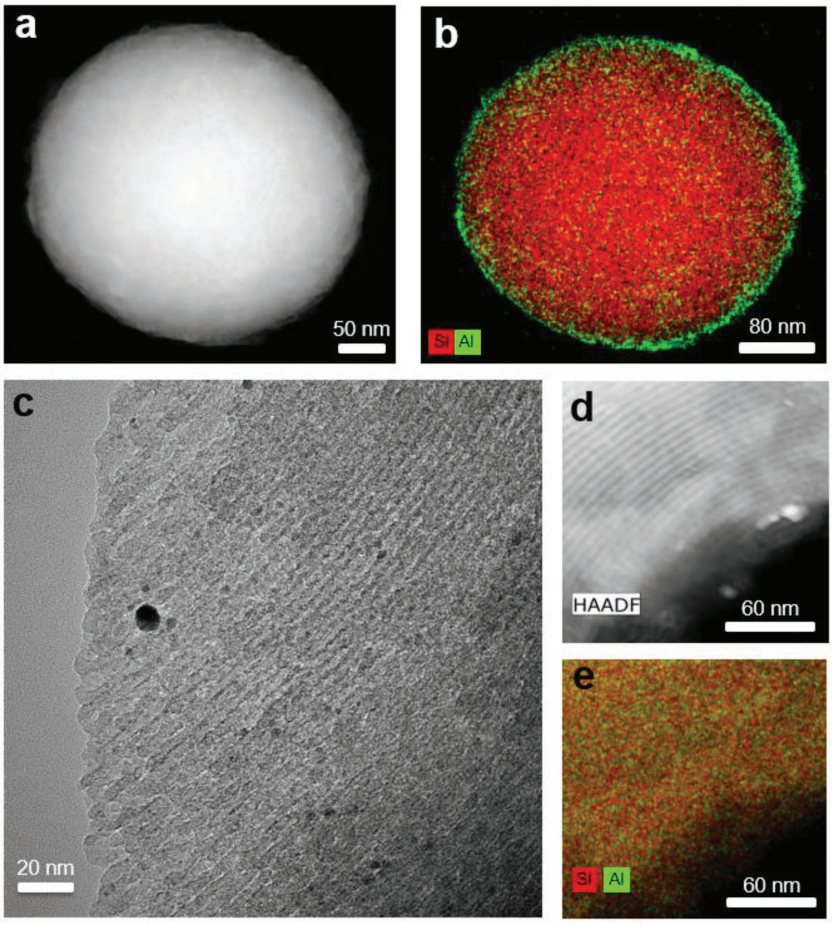

Figure 2. TEM and STEM images of C-Al_2O_3@SiO_2 a) under HAADF mode and b) with EDX mapping or c) C-Al_2O_3@2%Pt/SBA-15 d) under HAADF mode and e) with EDX mapping.

2.3. Deposition of Al_2O_3 by Nonhydrolytic Sol–Gel Chemistry

After depositing an amount of precursor corresponding to 40 monolayers of Al_2O_3 on SiO_2 spheres, the formation of a rough surface was observed by STEM (**Figure 3**a). EDX mapping revealed a conformal alumina overcoat with an average thickness 12 ± 4 nm, which corresponded to a monolayer thickness of about 0.3 nm. The coating of 2%Pt/SBA-15 was also performed and 3.4 mmol $g_{catalyst}^{-1}$ of Al was injected (corresponding to a coverage of 1.3 monolayer for Al(^{s}BuO)Br_2), which was the same molar amount as the aforementioned C-Al_2O_3@2%Pt/SBA-15 material (though corresponding to fewer monolayer). Similar to the materials obtained using our chelating method, deposition with NHSG chemistry did not alter the SBA-15 morphology (Figure 3c,d) and the characteristic XRD peaks of SBA-15 (Figure S2b, Supporting Information). The uniform mixture of SiO_2 and Al_2O_3 observed by EDX (Figure 3e) again suggested that alumina was deposited inside the pores, which was further supported by the reduced average pore diameter from 6.8 to 6.6 nm (Figure S2a, Supporting Information). We then estimated that the thickness formed by one monolayer equivalent of Al(^{s}BuO)Br_2 to be roughly 0.075 nm of alumina overcoat, which was comparable but slightly denser than what was obtained for C-Al_2O_3@2%Pt/SBA-15. This thickness was a similar order of magnitude albeit below that of N-Al_2O_3@SiO_2. This difference could either be due to the fact that our imaging method did not allow us to measure an overcoat thickness measurement as precisely as through physisorption, or that the initial micropore filling in SBA-15 skewed the pore size measurement by not contributing to the reduction of pore diameters in the mesopore range.

Compared to the chelation method, the overall concentration of the precursor loaded in the syringe was particularly important for controlling the Al_2O_3 growth during NHSG-based overcoating. Since the condensation was initiated by the higher temperature in the reaction flask, we found that the hot vapor generated during reflux caused the undesired gelation of precursor droplets before they dripped into the substrate suspension. When the total aluminum concentration in the syringe was set below 0.1 M, this early gelation did not occur anymore. With this adjustment, we were able to avoid any uncontrolled growth of Al_2O_3 outside the pore structure of SBA-15 (Figure S4, Supporting Information). It is also worth mentioning that the thickness of Al_2O_3 overcoats on 2%Pt/SBA-15 produced with the NHSG method were thinner then that prepared by the chelation method when the same molar amount of Al was injected (Figure S2a, Supporting Information). Such difference likely resulted from the less bulky NHSG precursor (Figure 1c), which could lead to a denser deposited monolayer. We further investigated the physical properties of these overcoats by analyzing the overcoated silica spheres, which allowed us to more accurately probe the overcoat texture and thickness by microscopy. Because the overcoat on C-Al_2O_3@SiO_2 was thinner than that of N-Al_2O_3@SiO_2, silica spheres with a thicker alumina coating were prepared for analysis (C9nm-Al_2O_3@SiO_2, the synthesis conditions are given in Section S1, Supporting Information). Physisorption results (Figure S5, Supporting Information) suggested that the pore volume of C9nm-Al_2O_3@SiO_2 was three times higher than that of N-Al_2O_3@SiO_2 (0.11 and 0.03 $cm^3\ g^{-1}$, respectively), which confirmed that two overcoating routes lead to different Al_2O_3 structural properties. We suggested that is not only due to the different steric hindrances of precursors but also the differences in condensation chemistry and growing mechanisms. We hypothesized that the rapid initial grafting reaction between Al(^{s}BuO)Br_2 and surface hydroxyl groups could ensure consecutive surface condensations, leading to a denser alumina network. On the other hand, Al(^{s}BuO)$_2$(EAA) may proceed through an oligomer deposition mechanism. Specifically, the precursors start polymerizing into sub-nanometer oligomers (sols) when injected into catalyst suspension. These sols gradually crosslink and heterogeneous nucleation may only happen when supersaturation is reached by progressive injection. Our previous coarse grain modeling

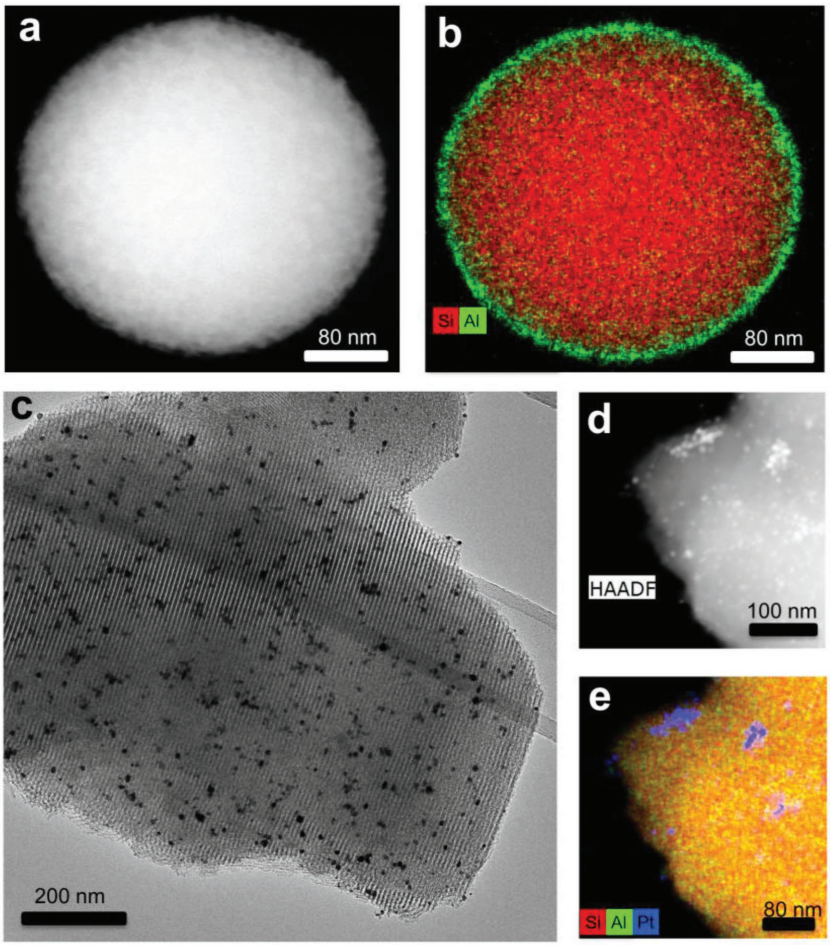

Figure 3. TEM and STEM images of N-Al_2O_3@SiO_2 a) under HAADF mode and b) with EDX mapping or c) N-Al_2O_3@2%Pt/SBA-15 d) under HAADF mode and e) with EDX mapping.

studies showed that the preferred mechanism of Al_2O_3 deposition in liquid phase using Al(^{s}BuO)$_3$ occurs via an oligomer deposition mechanism, where the alumina overcoat formed by the polymerization of alumina oligomers instead of monomeric precursors.[33] If the formation of alumina by the chelation method did indeed proceed through this oligomer-deposition mechanism, this would likely lead to a much more porous framework.

2.4. Improving the Stability of Cu/Al_2O_3 for Furfural Hydrogenation

As we and others have shown, deposition of a metal oxide overcoat onto a supported heterogeneous catalyst can stabilize the metal nanoparticles against sintering.[6,14,34–36] However, stabilization is only successful if the overcoat is conformal and successfully covers all of the metal nanoparticles. Herein, we use furfural hydrogenation, which is a copper-based industrially relevant reaction for producing furfural alcohol (FFA), to investigate the stability of an overcoated copper catalyst and, indirectly, measure the quality and conformality of the coating. Previously, we had also developed a layer-by-layer alumina overcoating method achieved by alternately reacting substrate with stoichiometric amounts of Al(^{s}BuO)$_3$ and H_2O and applied it to the same reaction.[28] Although that method also stabilized Cu/Al_2O_3, it was only able to stabilize the Cu on Al_2O_3 with low S_{BET} (45 m^2 g^{-1}) as the use of this method on the high surface area Al_2O_3 led to no discernable stabilization (Figure S6, Supporting Information), which limits the applicability of our prior method to less industrially relevant supports. Our first attempts to deposit Al_2O_3 using NHSG method leached all the copper out during the coating procedure, presumably due to the presence of the corrosive HBr byproduct. Therefore, we used the chelated Al(^{s}BuO)$_3$ precursor for overcoating Cu/Al_2O_3 to synthesize C-Al_2O_3@Cu/Al_2O_3 and demonstrate the benefit of having several available methods to slow down precursor condensation kinetics. Although in initial tests, we had found that EAA interacted with metallic copper and caused leaching (the color of reaction media turned blue after overcoating) during the coating process, this issue was easily resolved by oxidizing the copper with a mild thermal treatment before overcoating. With this pretreatment, the color change was not observed anymore. The S_{BET} of the resulting C-Al_2O_3@Cu/Al_2O_3 slightly decreased to 144 from 154 m^2 g^{-1}. The loading of Cu was determined inductively coupled plasma optical emission spectrometry (ICP-OES) and it was reduced from 5.0 to 2.4 wt%, as a result of the additional weight of Al_2O_3 in the overcoat. Based on N_2O chemisorption, the original number of Cu surface sites on Cu/Al_2O_3 was 53.6 µmol g^{-1} whereas no surface Cu sites were detected in the as-synthesized C-Al_2O_3@Cu/Al_2O_3. However, Cu sites could be re-exposed by calcination, after which 9.9 µmol g^{-1} of Cu surface sites was measured. This re-exposure of copper could be attributed to either pore formation by overcoat crystallization or the removal of residual precursor ligands strongly bound on the metal particles.[8,14] If all the active sites were re-exposed, the number of Cu surface sites should be roughly 25.7 µmol g^{-1} because of the reduced Cu loading. Therefore, ≈38% of active sites were recoverable after overcoating.

The uncoated and overcoated catalysts were then used to catalyze furfural hydrogenation in a fixed-bed flow reactor (**Figure 4**). In both cases, coke formation led to rapid deactivation of the catalyst, which could be partially reversed. However, the sintering of Cu particles during calcination and the liquid phase reaction could cause irreversible deactivation. The activity of Cu/Al_2O_3 was not fully recovered after calcination (Figure 4a), whereas the deactivation of C-Al_2O_3@Cu/Al_2O_3 could be completely reversed (Figure 4b). The spent catalysts were analyzed by TEM (Figure S7, Supporting Information) and significant particle sintering was observed on Cu/Al_2O_3. In contrast, most of the Cu particles in C-Al_2O_3@Cu/Al_2O_3 were still well dispersed after five catalytic cycles, which can be ascribed

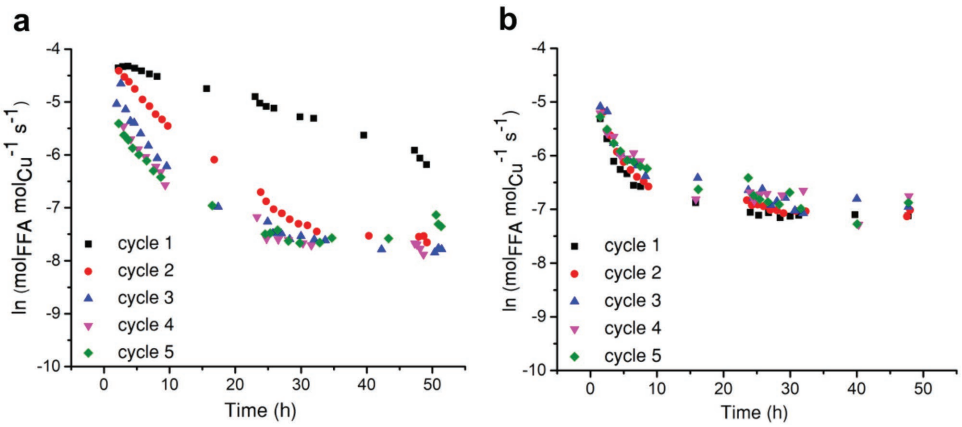

Figure 4. Results of continuous furfural hydrogenation over a) Cu/Al_2O_3 and b) $C\text{-}Al_2O_3@Cu/Al_2O_3$.

to the physical barrier formed by the protective Al_2O_3 overcoat. These results suggested that the chelation chemistry-based approach works on a broader range of supports compared to previous methods, which underlines the importance of slowing condensation kinetics. Accordingly, we consider chelation-based overcoating to be an easily performed but powerful method for overcoating a large array of supported metal catalysts, including those containing less leaching-resistant base metals.

2.5. Improving the Selectivity of Pt/SBA-15 for 4-Propylguaiacol Hydrodeoxygenation

To test the potential of our overcoats for improving catalyst activity, we tested our materials for the hydrodeoxygenation (HDO) of lignin-derived propyl guaiacol. Lignin is a plant fraction that is a polymer of phenylpropanoid subunits. Because of its aromatic-rich and energy dense structure, lignin is one of the most promising potential sources of chemicals and drop-in fuels to be derived from biomass.[37,38] However, the molecules that can be directly produced from lignin contain too much oxygen to be used directly as a fuel.[39] A typical example of such a molecule is propyl guaiacol, which we and others have produced as a majority product from softwood and, as the second most abundant product from hardwood lignin.[40–43] Hydrodeoxygenation of this molecule (and closely related ones) is a typical route for obtaining high quality fuels from lignin. In these reactions, the synergistic effects between metal and acid sites play an important role and a variety of bifunctional catalysts for catalytic upgrading of oxygenated phenolic molecules have been reported.[20,44–47] Although zeolites are an industrially relevant support, having abundant acid sites and high surface area, their hydrothermal stability is an issue for widespread use in biomass upgrading due to the amount of water that is generally present in such streams. Furthermore, their small pore size limits the diffusion of several molecules including lignin-derived oligomers and even some monomers.[45] Hence, creating acid sites on mesoporous SBA-15 supported metal catalysts would be an interesting application of Al_2O_3 overcoating method for synthetizing a stable bifunctional catalyst with a larger pore size for lignin valorization.

The HDO of 4-propylguaiacol was studied over a series of overcoated and uncoated Pt-based catalysts. Our HDO reaction temperature was somewhat lower compared to most (though not all) reported HDO conditions of lignin model compounds (typically above 200 °C)[48–50] to ensure that the pore structure of SBA-15 remains stable (TEM images of spent catalysts were shown in Figure S8, Supporting Information). Among all catalysts we synthesized, uncoated 2%Pt/SBA-15 had the highest rate in converting 4-propylguaiacol (**Figure 5**a), likely because of its greater number of accessible Pt sites (**Table 1**). Full conversion was reached after 3 h of reaction. Nevertheless, it had the lowest selectivity to fully deoxygenated products and the main product was 2-methoxy-4-propylcyclohexanol, which resulted only from ring hydrogenation. The selectivity of this product was 61% at a conversion of 59% and decreased with increasing conversion. However, increasing conversion only yielded 4-propylcyclohexanol and very small amount of fully deoxygenated C_9 alkane (propylcyclohexane), which indicated its limited HDO activity. Replacing the SBA-15 support with Al_2O_3 only slightly improved the selectivity to propylcyclohexane (≈40%) because the Lewis acidity facilitated HDO. Interestingly, the two differently overcoated catalysts displayed very different selectivities. $C\text{-}Al_2O_3@2\%Pt/SBA\text{-}15$ led to a similar propylcyclohexane selectivity to Pt/Al_2O_3 and other products like 1-propylcyclohexene and 4-propylcyclohexanone were also detected (the yields of these minor products are shown in Table S1, entry 7, Supporting Information), indicating that the overcoat prepared using the chelation method did not improve deoxygenation selectivity. In contrast, $N\text{-}Al_2O_3@2\%Pt/SBA\text{-}15$ showed a significantly enhanced propylcyclohexane selectivity (80%). $N\text{-}Al_2O_3@2\%Pt/SBA\text{-}15$ did display a slightly lower conversion (77%) at the same reaction time compared to $C\text{-}Al_2O_3@2\%Pt/SBA\text{-}15$, which was attributed to its reduced number of accessible Pt sites as determined by CO chemisorption (Table 1). Notably, using $N\text{-}Al_2O_3@2\%Pt/SBA\text{-}15$ led to a yield of about 10% aromatic products (4-propylphenol and propylbenzene). The selectivities toward these aromatic products were decreased when full conversion was reached, where the selectivity toward propylcyclohexane was close to 90% (Table S1, entry 6, Supporting Information). The production of aromatics suggests that the reaction proceeds through aromatic intermediates when $N\text{-}Al_2O_3$ overcoat is present. In comparison, selectivities to aromatic products were always less than 2.5% at the same reaction time when the other three

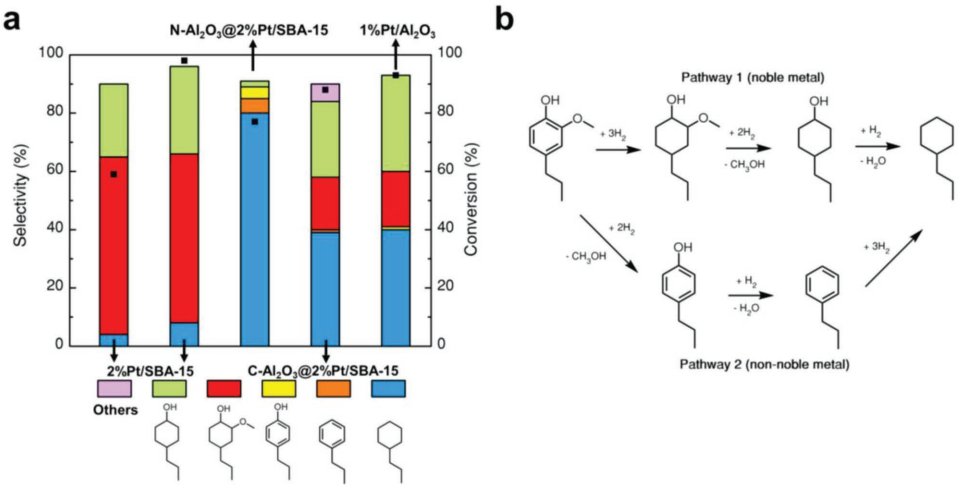

Figure 5. a) Selectivities and conversions of 4-propylguaiacol HDO over Pt based catalysts. The reaction time was 3 h and the amounts of catalysts were all 20 mg except for 1%Pt/Al_2O_3 (40 mg, due to its metal loading being only half of 2%Pt/SBA-15). The first bar on the left represents the low conversion result for 2%Pt/SBA-15. The conditions for these data were a reaction time of 1.5 h and a fivefold loading of 4-propylguaiacol substrate. Products listed as Others included 1-propylcyclohexene and 4-propylcyclohexanone. b) Reaction pathways of 4-propylguaiacol HDO.

catalysts were used. As has been previously reported, when using noble metal based catalyst, the benzene ring of 4-propylguaiacol is rapidly hydrogenated as the first step and subsequent deoxygenation occurs (Figure 5b, pathway 1), which is in agreement to our observations.[47,48] On the other hand, transition metal catalysts can catalyze the hydrogenolysis of C—O bonds first and then the hydrogenation of aromatic ring. However, even when this occurs, this pathway is much less favored than the alternate.[50] The majority of aromatic intermediates that were produced in the case of N-Al_2O_3@2%Pt/SBA-15 indicates that the C—O cleavage mechanism might be the primary one over this particular catalyst. However, no conversion was observed when the reaction was run under N_2 with this catalyst (Table S1, Supporting Information), which means that any HDO still required an H_2 environment to proceed.

2.6. The Effects of Physical and Chemical Properties of Overcoats on Hydrodeoxygenation

Pt particles and surface acid sites have previously been reported to have a synergistic effect during hydrodeoxygenation.[45,47,51] The catalyst with the most to the fewest acid sites per unit surface area were 2%Pt/Al_2O_3 > N-Al_2O_3@2%Pt/SBA-15 > C-Al_2O_3@2%Pt/SBA-15 (Table 1). However, the deoxygenation activity did not follow the same trend as N-Al_2O_3@2%Pt/SBA-15 showed the highest selectivity toward fully deoxygenated alkanes compared to other catalysts. Powder XRD analyses confirmed the amorphous nature of alumina overcoats produced from both methods (Figure S9, Supporting Information). According to the shift of the Si—OH band at 3745 cm^{-1} to the Al—OH band at 3739 cm^{-1} in the fourier-transform infrared (FTIR) spectra and the shifts as well as the broadenings of the proton signals in the ^1H magic angle spinning solid-state nuclear magnetic resonance (ssNMR) spectra (Figures S10 and S11, Supporting Information), we concluded that the surfaces of both N-Al_2O_3@2%Pt/SBA-15 and C-Al_2O_3@2%Pt/SBA-15 were fully covered by Al_2O_3.[52] Additionally, diffuse reflectance infrared Fourier transform spectroscopy with a pyridine probe (pyridine-DRIFT) suggested that both overcoated catalysts had stronger Lewis acid sites compared to 1%Pt/Al_2O_3 (Figure S12, Supporting Information). Therefore, the different selectivities of C-Al_2O_3@2%Pt/SBA-15 and N-Al_2O_3@2%Pt/SBA-15 seem to be unrelated to the crystal structure of alumina, degree of overcoat coverage and the strength of acidity. We performed ^{27}Al solid-state NMR to further elucidate the chemical compositions of two Al_2O_3 overcoats (**Figure 6**a). The octahedrally coordinated Al sites predominated in 1%Pt/Al_2O_3, which corresponds to the characteristic structure of γ-Al_2O_3. Interestingly, penta-coordinated

Table 1. Summary of the characterization data of Pt catalysts.

Catalyst	Al/Si ratio[a)]	S_{BET} [m^2 g^{-1}]	$V_{micropore}$ [cm^3 g^{-1}][b)]	Lewis acid sites [μmol m^{-2}][c)]	$Pt_{surface}$ [μmol g^{-1}]	d_{Pt} [nm][d)]
2%Pt/SBA-15	N/A	723	0.03	≈0	58.5	3.5 ± 2.4
N-Al_2O_3@2%Pt/SBA-15	0.50	449	0	1.3	9.4	3.8 ± 1.5
C-Al_2O_3@2%Pt/SBA-15	0.47	392	0.01	0.9	30.2	4.3 ± 2.6
1%Pt/Al_2O_3	N/A	164	0	1.5	35.2	5.0 ± 1.9

[a)]Determined by inductively coupled plasma optical emission spectrometry (XPS), using the signals of Si 2s and Al 2s; [b)]Estimated using the t-plot method; [c)]Determined by NH_3 temperature programmed desorption and the value of S_{BET}. Pyridine-DRIFT analysis (Figure S12, Supporting Information) suggested the absence of Brønsted acid site; [d)]Determined by TEM analysis.

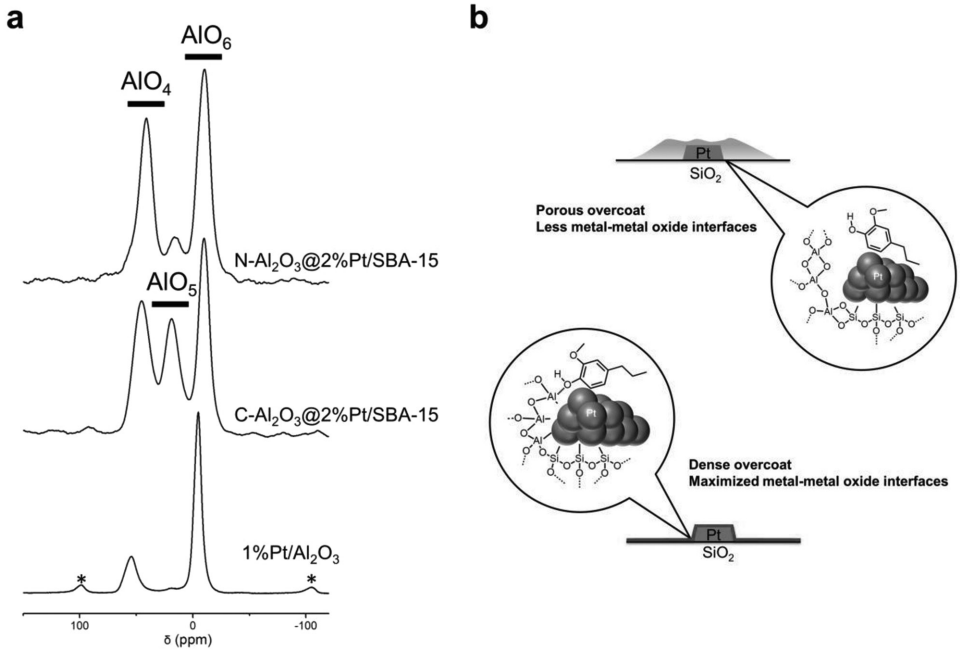

Figure 6. a) ^{27}Al solid-state NMR spectra of C-Al_2O_3@2%Pt/SBA-15, N-Al_2O_3@2%Pt/SBA-15, and 1%Pt/SBA-15. Spinning sidebands were labeled by asterisks. b) Schematic illustration of the effect of overcoat texture on the hydrodeoxygenation of 4-propylguaiacol.

coordinated Al sites were found in both overcoated catalysts. This Al (V) site is considered electron-deficient thus leading to a strong Lewis acidity,[53] which confirmed the pyridine-DRIFT results. Although the ratio of Al(V) and Al(IV) may differ in the two overcoated catalysts, we assumed and results confirmed that the alumina overcoats synthesized from Al(^{s}BuO)$_3$–$AlBr_3$ and Al(^{s}BuO)$_3$–EAA were chemically similar.

Many studies have suggested that the metal-support interface plays an important role in HDO.[20,44] A recent investigation on phenol HDO revealed a mechanism showing that direct deoxygenation can proceed by the first interaction between the phenol tautomer and an surface oxophilic site, followed by the hydrogenation of the carbonyl group and a final dehydration step to form benzene.[48] The presence of electron-deficient Al(V) sites in the alumina overcoat and aromatic products suggests that 4-propylguaiacol was converted in a similar direct deoxygenation pathway over N-Al_2O_3@2%Pt/SBA-15. Because Al(V) sites were present in both overcoated Pt/SBA-15, we attributed the different selectivities to the distinct structural (rather than chemical) properties of two overcoats. As discussed in 3.3, the Al_2O_3 overcoat prepared from chelation chemistry method is more porous. Such physical differences of overlayers can also explain the fact that the accessible Pt sites of C-Al_2O_3@2%Pt/SBA-15 outnumbered those of N-Al_2O_3@2%Pt/SBA-15 by a factor of 3 after overcoating despite their similar metal loadings (as determined by ICP-OES: 1.7% and 1.9%). Compared to C-Al_2O_3@2%Pt/SBA-15, the denser overlayer on N-Al_2O_3@2%Pt/SBA-15 led to increased intimate contact between Pt particles and Al_2O_3, which creates more interfacial metal-support active sites. In summary, with the more active overcoat, the 4-propyluaiacol was likely mainly anchored on the abundant Pt-Al(V) sites of N-Al_2O_3@2%Pt/SBA-15, which promoted initial deoxygenation/hydrogenolysis and subsequent ring hydrogenation to form cyclohexane. In contrast, on the C-Al_2O_3@2%Pt/SBA-15, 4-propylguaicaol likely had less interactions with the Pt-SiO_2–Al_2O_3 interfaces due to the higher porosity of the overcoat. Therefore, the reaction proceeded mostly through molecules bound directly to the metal (Figure 6b). In such cases, the dominant reaction is known to be ring hydrogenation. These HDO results exemplify the significant control that overcoat nanostructures can have on the selectivities of the reactions catalyzed by the corresponding heterogeneous catalyst.

3. Conclusions

We studied the formation of alumina overcoats over high surface area supported catalysts by slowing down the kinetics of alumina precursor condensation and developed two distinct approaches to achieve this kinetic control. In one case, we used nonhydrolytic sol–gel chemistry and in the other we used a chelation agent to manipulate the hydrolysis/condensation kinetics of Al(^{s}BuO)$_3$. Both methods were easy to conduct, yet highly versatile, allowing us to deposit conformal alumina overcoats onto various high surface area substrates with subnanometer precision. However, both methods offered distinct features that were advantageous in different cases. The nonhydrolytic route produced a denser Al_2O_3 overcoat and could drastically improve the catalyst's selectivity during lignin hydrodeoxygenation—a reaction for which, the metal–metal oxide interface plays an important role. However, the nonhydrolytic sol–gel method could not be used with a supported base metal catalyst like Cu because it lead to metal leaching during the coating procedure. In this case, the Al_2O_3 overcoat prepared with chelation chemistry was the only one that could produce a conformal overcoat and protect the metal nanoparticles against sintering during liquid phase hydrogenation. Moreover, both

methods create stronger Lewis acid sites compared to γ-Al_2O_3 according to pyridine-DRIFT and SSNMR analyses. These differing characteristics provide an especially versatile toolbox for renewable chemistry where stability and selectivity is especially important in the presence of water in and numerous oxygen functionalities in the reactants. At the same time, the high degree of control over the overcoat thickness and texture could allow the tailoring of the surface nanostructures to several materials that are used in applications beyond heterogeneous catalysis.

4. Experimental Section

Chemicals and Materials: All chemicals were analytical grade and obtained from commercial suppliers. They were used without further purification unless stated otherwise. Air and moisture-sensitive reagents were handled using a nitrogen filled glove box and a standard Schlenk line apparatus. TEOS, tetramethyl orthosilicate (TMOS), $AlBr_3$, CaH_2, $H_2PtCl_6 \cdot 6H_2O$, furfural, and 1-butanol were obtained from Acros. Benzophenone, magnesium, sodium, Pluronic 123 (P123), 3-propylguaiacol, 2,2,4-trimethylpentane (isooctane), CH_2Br_2, EAA, 2-butanol and $HNO_{3(aq)}$ (≈68%) were purchased from Sigma-Aldrich. Molecular sieve (4 Å), $Al(^sBuO)_3$, and $HCl_{(aq)}$ (≈37%) were obtained from Merck. Ethanol and diethyl ether were obtained from Fisher Scientific. Silicon carbide (100 mesh) was obtained from Strem. $Cu(NO_3)_2 \cdot 3H_2O$ was obtained from ABCR. $NH_{3(aq)}$ (≈25%) was purchased from VWR Chemicals. γ-Al_2O_3 (Pural SB) was obtained from Sasol. Diethyl ether was dried over Na-benzophenone, distilled and stored over molecular sieves. 2-butanol was dried over Mg, distilled, and stored over molecular sieves. CH_2Br_2 was dried over CaH_2, distilled, and stored over molecular sieves. Furfural and EAA were purified by distillation under reduced pressure. The water used in this study was purified by a Millipore Milli-Q Advantage A10 water purification system resulting in a resistivity higher than 18 MΩ cm. All gases were purchased from Carbagas.

Preparation of Supports and Catalysts: The silica spheres were synthesized by the Stöber method.[54] Typically, 3.8 mL of TEOS, 7.7 mL NH_3 (≈25%), and 18 mL of deionized water were mixed with 120 mL ethanol. The mixture was stirred and reacted at room temperature for 24 h. The product was centrifuged and washed three times first with ethanol then water. SBA-15 was synthesized based on a previously published method that was slightly modified.[55] Briefly, 2.8 g of Pluronic P-123 was dissolved in 104 g of 1.6 M $HCl_{(aq)}$ by vigorous stirring. Then, 4 mL of TMOS was slowly added and the resulting mixture was stirred for 24 h. The suspension was transferred into a Teflon lined stainless steel autoclave and heated at 110 °C for 24 h. After the hydrothermal treatment, the remaining surfactant was removed by ethanol using a standard Soxhlet apparatus for 24 h. All synthetized supports were calcined at 500 °C for 5 h under flow of synthetic air (ramping rate: 2 °C min^{-1}) and dried under reduced pressure (below 10^{-2} bar) at 120 °C prior to impregnation.

Cu/Al_2O_3 (5%) was prepared by incipient wetness impregnation using $Cu(NO_3)_2 \cdot 3H_2O$ dissolved in 0.1 M $HNO_{3(aq)}$ as the precursor and calcined γ-Al_2O_3 as the support. The impregnated powder was subsequently dried in an oven at 105 °C overnight and reduced at 300 °C for 5 h by flowing H_2 (ramping rate: 1 °C min^{-1}). 2%Pt/SBA-15 was prepared by incipient wetness impregnation using $H_2PtCl_6 \cdot 6H_2O$ dissolved in 1 M $HCl_{(aq)}$ as the precursor. The impregnated powder was dried overnight at 105 °C, calcined at 400 °C for 3 h and then reduced at 300 °C for 3 h. Both 1% Pt/Al_2O_3 and 2% Pt/SBA-15 were prepared with this procedure.

Catalyst Overcoating—NHSG-Based Approach: All catalysts (0.5 g) were dried overnight under reduced pressure prior to overcoating. The precursor was prepared by dissolving $AlBr_3$ and $Al(^sBuO)_3$ in 20 mL CH_2Br_2. The precursor solution was loaded into a glass syringe (Hamilton US) with a Teflon plunger. The syringe needle was positioned into the reaction flask containing catalyst suspension refluxing at 100 °C and an automatic syringe pump (KDS 100 legacy syringe pump) was used to control the injection rate. SiO_2 spheres were dispersed in 10 mL CH_2Br_2 and then overcoated by injecting a precursor solution comprising 0.08 mL $Al(^sBuO)_3$ and 0.17 g $AlBr_3$. The injection rate was adjusted to 0.5 mL h^{-1}, which correspond to one monolayer amount of precursor per hour. The solution was left to react for 24 h after the injection was completed. 2%Pt/SBA-15 was dispersed in 20 mL CH_2Br_2 and coated by injecting a precursor solution containing 0.14 mL $Al(^sBuO)_3$ and 0.3 g $AlBr_3$ at a rate of 1 mL h^{-1}. The solution was left to react for 6 h after the injection was completed. In both cases the following two subsequent postsynthesis treatments followed: first, 20 mL of diethyl ether were added into the suspension to quench highly reactive residual Al–Br groups. The solution was then kept stirring at 80 °C overnight. The crude products were centrifuged and sequentially washed twice with diethyl ether, ethanol, and water. After washing, the samples were stirred in 0.1 M $NH_{3(aq)}$ at 60 °C overnight. The products were washed with water and dried in a vacuum oven at 60 °C. Subsequently, the crude was reacted with 0.1 M $NH_{3(aq)}$, washed thoroughly and calcined at 500 °C to completely remove the byproduct HBr. Finally, Overcoated Pt/SBA-15 was reduced at 300 °C for 3 h prior to the catalytic reaction. The resulting materials are referred to as N-Al_2O_3@2%Pt/SBA-15 and N-Al_2O_3@SiO_2 below.

Catalyst Overcoating—Chelation Chemistry-Based Approach: C-Al_2O_3@SiO_2: SiO_2 spheres (0.5 g) were dispersed in a mixture containing 25 mL ethanol, 0.04 mL of 25 wt% $NH_{3(aq)}$ and 1 mL H_2O. The precursor solution was prepared by stirring 0.13 mL $Al(^sBuO)_3$ and 0.05 mL EAA in 9.8 mL of 2-butanol for 1 h. This precursor solution was then injected into the mixture containing silica spheres using the aforementioned syringe setup at a rate of 1 mL h^{-1}. The suspension was stirred at room temperature for 8 h after the injection.

C-Al_2O_3@Cu/Al_2O_3: Cu/Al_2O_3 was preoxidized at 250 °C for 2 h by flowing synthetic air before overcoating. Then, 0.5 g of CuO/Al_2O_3 was dispersed in the same solution as described above. The precursor solution was prepared by stirring 2 mL $Al(^sBuO)_3$ and 0.8 mL EAA in 27.2 mL 2-butanol for 1 h. This precursor solution was then injected into the mixture containing the substrate at a rate of 1 mL h^{-1}. The suspension was heated to 40 °C and stirred for 6 h after the injection.

C-Al_2O_3@2%Pt/SBA-15: The uncoated catalyst (0.5 g of 2%Pt/SBA-15) was dispersed in a mixture containing 25 mL ethanol, 0.02 mL 25 wt% NH_3, and 1 mL H_2O. The precursor solution was prepared by stirring 0.44 mL $Al(^sBuO)_3$ and 0.165 mL EAA in 9.4 mL 2-butanol for 1 h. The precursor was then injected into the mixture containing the substrate at a rate of 1 mL h^{-1}. The solution was left to react at room temperature and stirred for 8 h after the injection.

All the overcoated samples were washed three times with ethanol followed by water and then dried in a vacuum oven at 60 °C. Both overcoated catalysts (C-Al_2O_3@Cu/Al_2O_3 and C-Al_2O_3@Pt/SBA-15) were further calcined at 400 °C for 3 h and reduced at 300 °C for 5 h. The additional materials synthesis details and description of characterization techniques are shown in Sections S1 and S2 in the Supporting Information, respectively.

Catalytic Activity Tests—Hydrodeoxygenation of a Model Lignin Monomer: The catalyst was mixed with 10.5 mL isooctane and 0.1 mL 4-propylguaiacol in a 25 mL stainless-steel reactor (Parr). The reactions were stirred at 600 rpm under 15 bar H_2 at 200 °C. The actual pressure after the temperature rising to 200 °C was ≈25 bar. The reaction time and the amounts of reactants were varied to reach different conversions. The temperature was ramped up with a heating plate and heating tape controlled by an Omega Proportional-Integral-Derivative controller. The product was analyzed by an Agilent Technologies 7890 A gas chromatography apparatus equipped with a flame ionization detector (GC-FID) and an HP-5 column (50 m, 0.32 mm). The products were quantified using calibration curves obtained prepared with authenticated standards except for 2-methoxy-4-propylcyclohexanol and 4-propylcyclohexanol. These two products were quantified using the effective carbon number method with *n*-decane as an internal standard, which has proven to be accurate for lignin-derived monomers.[40]

External diffusion limitations were assumed to be negligible based on experiments where the stirring speed was varied and internal diffusion limitations were assumed to be negligible based on our calculation of the Weisz–Prater criterion (see Section S4, Supporting Information).

Catalytic Activity Tests—Hydrogenation of Furfural: Furfural hydrogenation was performed using a stainless steel fixed-bed down flow tubular reactor with an inner diameter 4.5 mm, which was previously described.[28] The catalytic bed was prepared by mixing the catalysts with SiC and immobilized in the metal tube between two quartz wool plugs. The remainder of the tube was filled with SiC and both ends were plugged with quartz wool. The heated zone corresponding to the area containing the catalytic bed was delimited by two external conductive stainless-steel blocks enclosed in a furnace. Before the first run, the catalyst was reduced under H_2 flow (100 mL min^{-1}) for 5 h at 300 °C. After cooling down to the reaction temperature (130 °C), hydrogen flow was adjusted to 35 mL min^{-1} using a Brooks mass flow controller and pressure was set to 23 bar using a back pressure regulator (Tescom). A furfural solution (70 g kg^{-1} in 1-butanol) was fed into the reactor using SSI Series II high-performance liquid chromatography (HPLC) pump at a rate of 0.10 mL min^{-1}. Liquid samples were collected using a Jerguson gage equipped with a needle valve and analyzed by GC-FID. The products were quantified by the calibration curves obtained using standard chemicals. Periodically, furfural flow was stopped and the catalyst was regenerated by calcination at 400 °C for 1 h (under a flow of synthetic air at 100 mL min^{-1}) and reduction at 300 °C for 5 h (under a flow of H_2 at 100 mL min^{-1}). Catalytic activities were evaluated by the yield of furfural alcohol per unit time and mol of Cu. The internal diffusion limitation was assumed to be negligible based on our calculation of the Weisz–Prater criterion (see Section S4, Supporting Information).

Supporting Information

Supporting Information is available from the Wiley Online Library or from the author.

Acknowledgements

This work was supported by the European Research Council (ERC) under the European Union's Horizon 2020 research and innovation program (Starting grant: CATACOAT, No. 758653), the Swiss National Science Foundation through grant PYAPP2_154281 and by EPFL. This work was also accomplished within the framework of the Swiss Competence Center for Bioenergy Research (SCCER-BIOSWEET). The authors thank Benjamin Le Monnier for purifying ethyl acetoacetate and aluminum sec-butoxide. The authors thank the EPFL interdisciplinary center for electron microscopy for support during electron microscopy measurements. The authors thank Emilie Baudat and Pierre Mettraux for their help in performing measurements with ssNMR and XPS, respectively. The authors thank EPFL's central environmental laboratory for the ICP-OES measurements.

Conflict of Interest

The authors declare no conflict of interest.

Keywords

alumina, catalyst stability, heterogeneous catalysis, hydrodeoxygenation, nanostructured catalysts

Received: May 4, 2018
Revised: June 21, 2018
Published online:

[1] Q. Zhang, I. Lee, J. B. Joo, F. Zaera, Y. Yin, *Acc. Chem. Res.* **2013**, *46*, 1816.
[2] F. Héroguel, B. Rozmysłowicz, J. S. Luterbacher, *CHIMIA Int. J. Chem.* **2015**, *69*, 582.
[3] H. N. Pham, A. E. Anderson, R. L. Johnson, T. J. Schwartz, B. J. O'Neill, P. Duan, K. Schmidt-Rohr, J. A. Dumesic, A. K. Datye, *ACS Catal.* **2015**, *5*, 4546.
[4] B. J. O'Neill, D. H. K. Jackson, J. Lee, C. Canlas, P. C. Stair, C. L. Marshall, J. W. Elam, T. F. Kuech, J. A. Dumesic, G. W. Huber, *ACS Catal.* **2015**, *5*, 1804.
[5] H. Yang, Y. Chong, X. Li, H. Ge, W. Fan, J. Wang, *J. Mater. Chem.* **2012**, *22*, 9069.
[6] J. Lu, B. Fu, M. C. Kung, G. Xiao, J. W. Elam, H. H. Kung, P. C. Stair, *Science* **2012**, *335*, 1205.
[7] S. H. Joo, J. Y. Park, C.-K. Tsung, Y. Yamada, P. Yang, G. A. Somorjai, *Nat. Mater.* **2009**, *8*, 126.
[8] H. Zhu, Z. Ma, S. H. Overbury, S. Dai, *Catal. Lett.* **2007**, *116*, 128.
[9] S.-C. Shen, S. Kawi, *J. Phys. Chem. B* **1999**, *103*, 8870.
[10] N. Pham, A. E. Anderson, R. L. Johnson, K. Schmidt-Rohr, A. K. Datye, *Angew. Chem., Int. Ed.* **2012**, *51*, 13163.
[11] X. She, J. H. Kwak, J. Sun, J. Hu, M. Y. Hu, C. Wang, C. H. F. Peden, Y. Wang, *ACS Catal.* **2012**, *2*, 1020.
[12] A. C. Alba-Rubio, B. J. O'Neill, F. Shi, C. Akatay, C. Canlas, T. Li, R. Winans, J. W. Elam, E. A. Stach, P. M. Voyles, J. A. Dumesic, *ACS Catal.* **2014**, *4*, 1554.
[13] J. Lu, B. Liu, J. P. Greeley, Z. Feng, J. A. Libera, Y. Lei, M. J. Bedzyk, P. C. Stair, J. W. Elam, *Chem. Mater.* **2012**, *24*, 2047.
[14] B. J. O'Neill, D. H. K. Jackson, A. J. Crisci, C. A. Farberow, F. Shi, A. C. Alba-Rubio, J. Lu, P. J. Dietrich, X. Gu, C. L. Marshall, P. C. Stair, J. W. Elam, J. T. Miller, F. H. Ribeiro, P. M. Voyles, J. Greeley, M. Mavrikakis, S. L. Scott, T. F. Kuech, J. A. Dumesic, *Angew. Chem., Int. Ed.* **2013**, *52*, 13808.
[15] J. Lu, J. W. Elam, P. C. Stair, *Acc. Chem.Res.* **2013**, *46*, 1806.
[16] M. Leskelä, M. Ritala, *Angew. Chem., Int. Ed.* **2003**, *42*, 5548.
[17] R. A. Caruso, M. Antonietti, *Chem. Mater.* **2001**, *13*, 3272.
[18] F. Babonneau, L. Coury, J. Livage, *J. Non-Cryst. Solids* **1990**, *121*, 153.
[19] Z. Teng, G. Zheng, Y. Dou, W. Li, C.-Y. Mou, X. Zhang, A. M. Asiri, D. Zhao, *Angew. Chem., Int. Ed.* **2012**, *51*, 2173.
[20] F. Héroguel, L. Silvioli, Y.-P. Du, J. S. Luterbacher, *J. Catal.* **2018**, *358*, 50.
[21] R. Nass, H. Schmidt, *J. Non-Cryst. Solids* **1990**, *121*, 329.
[22] A. Mitra, G. De, *Langmuir* **2014**, *30*, 15292.
[23] S. Acosta, R. J. P. Corriu, D. Leclercq, P. Lefèvre, P. H. Mutin, A. Vioux, *J. Non-Cryst. Solids* **1994**, *170*, 234.
[24] P. Arnal, R. J. P. Corriu, D. Leclercq, P. H. Mutin, A. Vioux, *Chem. Mater.* **1997**, *9*, 694.
[25] A. Vioux, *Chem. Mater.* **1997**, *9*, 2292.
[26] L. Bonhomme-Coury, F. Babonneau, J. Livage, *J. Sol-Gel Sci. Technol.* **1994**, *3*, 157.
[27] S. Kurajica, J. Popović T. G. Kraljević E. Tkalčec, I. Simčić, V. Mandić, A. Altomare, A. Moliterni, X. Rocquefelte, *J. Sol-Gel Sci. Technol.* **2014**, *71*, 217.
[28] F. Héroguel, B. P. Le Monnier, K. S. Brown, J. C. Siu, J. S. Luterbacher, *Appl. Catal., B* **2017**, *218*, 643.
[29] M. Baca, E. de la Rochefoucauld, E. Ambroise, J.-M. Krafft, R. Hajjar, P. P. Man, X. Carrier, J. Blanchard, *Microporous Mesoporous Mater.* **2008**, *110*, 232.
[30] C. M. A. Parlett, L. J. Durndell, A. Machado, G. Cibin, D. W. Bruce, N. S. Hondow, K. Wilson, A. F. Lee, *Catal. Today* **2014**, *229*, 46.
[31] P. Iengo, M. Di Serio, A. Sorrentino, V. Solinas, E. Santacesaria, *Appl. Catal,, A* **1998**, *167*, 85.
[32] C. P. Canlas, J. Lu, N. A. Ray, N. A. Grosso-Giordano, S. Lee, J. W. Elam, R. E. Winans, R. P. Van Duyne, P. C. Stair, J. M. Notestein, *Nat. Chem.* **2012**, *4*, 1030.

[33] K. S. Brown, C. Saggese, B. P. Le Monnier, F. Héroguel, J. S. Luterbacher, *J. Phys. Chem. C* **2018**, *122*, 6713.
[34] X. Liu, Q. Zhu, Y. Lang, K. Cao, S. Chu, B. Shan, R. Chen, *Angew. Chem.* **2017**, *129*, 1670.
[35] J. Lee, D. H. K. Jackson, T. Li, R. E. Winans, J. A. Dumesic, T. F. Kuech, G. W. Huber, *Energy Environ. Sci.* **2014**, *7*, 1657.
[36] E. D. Goodman, J. A. Schwalbe, M. Cargnello, *ACS Catal.* **2017**, *7*, 7156.
[37] J. S. Luterbacher, D. M. Alonso, J. A. Dumesic, *Green Chem.* **2014**, *16*, 4816.
[38] G. W. Huber, S. Iborra, A. Corma, *Chem. Rev.* **2006**, *106*, 4044.
[39] Q. Lu, W.-Z. Li, X.-F. Zhu, *Energy Convers. Manage.* **2009**, *50*, 1376.
[40] L. Shuai, M. T. Amiri, Y. M. Questell-Santiago, F. Héroguel, Y. Li, H. Kim, R. Meilan, C. Chapple, J. Ralph, J. S. Luterbacher, *Science* **2016**, *354*, 329.
[41] W. Lan, M. T. Amiri, C. M. Hunston, J. S. Luterbacher, *Angew. Chem. Int. Ed.* **2018**, *57*, 1356.
[42] I. Klein, B. Saha, M. M. Abu-Omar, *Catal. Sci. Technol.* **2015**, *5*, 3242.
[43] S.-F. Koelewijn, S. V. den Bosch, T. Renders, W. Schutyser, B. Lagrain, M. Smet, J. Thomas, W. Dehaen, P. V. Puyvelde, H. Witters, B. F. Sels, *Green Chem.* **2017**, *19*, 2561.
[44] A. M. Robinson, J. E. Hensley, J. W. Medlin, *ACS Catal.* **2016**, *6*, 5026.
[45] H. Lee, H. Kim, M. J. Yu, C. H. Ko, J.-K. Jeon, J. Jae, S. H. Park, S.-C. Jung, Y.-K. Park, *Sci. Rep.* **2016**, *6*, 28765.
[46] T. Nimmanwudipong, R. C. Runnebaum, D. E. Block, B. C. Gates, *Energy Fuels* **2011**, *25*, 3417.
[47] M. Hellinger, H. W. P. Carvalho, S. Baier, D. Wang, W. Kleist, J.-D. Grunwaldt, *Appl. Catal., A* **2015**, *490*, 181.
[48] P. M. de Souza, R. C. Rabelo-Neto, L. E. P. Borges, G. Jacobs, B. H. Davis, D. E. Resasco, F. B. Noronha, *ACS Catal.* **2017**, *7*, 2058.
[49] C. R. Lee, J. S. Yoon, Y.-W. Suh, J.-W. Choi, J.-M. Ha, D. J. Suh, Y.-K. Park, *Catal. Commun.* **2012**, *17*, 54.
[50] M. V. Bykova, D. Y. Ermakov, V. V. Kaichev, O. A. Bulavchenko, A. A. Saraev, M. Y. Lebedev, V. A. Yakovlev, *Appl. Catal. B* **2012**, *113–114*, 296.
[51] J. Horáček, G. Šťávová, V. Kelbichová, D. Kubička, *Catal. Today* **2013**, *204*, 38.
[52] M. Digne, P. Sautet, P. Raybaud, P. Euzen, H. Toulhoat, *J. Catal.* **2002**, *211*, 1.
[53] F. R. Chen, J. G. Davis, J. J. Fripiat, *J. Catal.* **1992**, *133*, 263.
[54] W. Stöber, A. Fink, E. Bohn, *J. Colloid Interface Sci.* **1968**, *26*, 62.
[55] A. Galarneau, H. Cambon, F. Di Renzo, F. Fajula, *Langmuir* **2001**, *17*, 8328.

